# BRAIN
A JOURNAL OF NEUROLOGY

# Exosome secretion is a key pathway for clearance of pathological TDP-43

Yohei Iguchi,[1,2] Lara Eid,[1,2] Martin Parent,[1,2] Geneviève Soucy,[1,2] Christine Bareil,[1,2] Yuichi Riku,[3] Kaori Kawai,[3] Shinnosuke Takagi,[3] Mari Yoshida,[4] Masahisa Katsuno,[3] Gen Sobue[3] and Jean-Pierre Julien[1,2]

Cytoplasmic TDP-43 aggregation is a pathological hallmark of amyotrophic lateral sclerosis and frontotemporal lobar degeneration. Here we investigated the role of exosomes in the secretion and propagation of TDP-43 aggregates. TDP-43 was detected in secreted exosomes from Neuro2a cells and primary neurons but not from astrocytes or microglia. Evidence is presented that protein aggregation and autophagy inhibition are factors that promote exosomal secretion of TDP-43. We also report that levels of exosomal TDP-43 full length and C-terminal fragment species are upregulated in human amyotrophic lateral sclerosis brains. Exposure of Neuro2a cells to exosomes from amyotrophic lateral sclerosis brain, but not from control brain, caused cytoplasmic redistribution of TDP-43, suggesting that secreted exosomes might contribute to propagation of TDP-43 proteinopathy. Yet, inhibition of exosome secretion by inactivation of neutral sphingomyelinase 2 with GW4869 or by silencing RAB27A provoked formation of TDP-43 aggregates in Neuro2a cells. Moreover, administration of GW4869 exacerbated the disease phenotypes of transgenic mice expressing human TDP-43[A315T] mutant. Thus, even though results suggest that exosomes containing pathological TDP-43 may play a key role in the propagation of TDP-43 proteinopathy, a therapeutic strategy for amyotrophic lateral sclerosis based on inhibition of exosome production would seem inappropriate, as *in vivo* data suggest that exosome secretion plays an overall beneficial role in neuronal clearance of pathological TDP-43.

1 Centre de recherche de l'Institut universitaire en santé mentale de Québec, Quebec City, Qc, Canada
2 Department of Psychiatry and Neuroscience, Université Laval, Quebec City, Qc, Canada
3 Department of Neurology, Nagoya University Graduate School of Medicine, Nagoya, Aichi, Japan
4 Department of Neuropathology, Institute for Medical Science of Aging, Aichi Medical University, Aichi, Japan

Correspondence to: Jean-Pierre Julien,
2601 Chemin de la Canardière,
Québec, QC, G1J 2G3 Canada
E-mail: jean-pierre.julien@fmed.ulaval.ca

## Introduction

Ubiquitinated cytoplasmic inclusions are a common pathological feature of amyotrophic lateral sclerosis (ALS) and frontotemporal lobar degeneration (FTLD-TDP). TDP-43 (encoded by *TARDBP*) has been known to be a major component of such inclusions (Arai *et al.*, 2006; Neumann *et al.*, 2006). TDP-43 is a nuclear RNA binding protein that redistributes from the nucleus to cytoplasm in affected neurons or glial cells (Arai *et al.*, 2006; Neumann *et al.*, 2006). TDP-43 C-terminal region represents glutamine/asparagine (Q/N) prion-like domain, and this low complexity domain

mediates self-aggregation (Blokhuis *et al.*, 2013; Budini *et al.*, 2015). Most of the disease-causative mutations of TDP-43 also localize in this region, increase own protein stability (Ling *et al.*, 2010; Watanabe *et al.*, 2013), and enhance its aggregation propensity (Johnson *et al.*, 2008, 2009).

An initial symptom of ALS commonly appears at a single focal lesion, and it horizontally or vertically spreads, as if a 'pathogen' contiguously or trans-synaptically transmits from cell to cell (Ravits and La Spada, 2009; Brettschneider *et al.*, 2014). The paradigm of prion-like propagation has been speculated as the cause of the spreading as well as other neurodegenerative diseases such as Alzheimer's disease or Parkinson's disease (Ling *et al.*, 2013; Falsone and Falsone, 2015; Maniecka and Polymenidou, 2015). Nonaka *et al.* (2013) demonstrated that an insoluble fraction of ALS or FTLD-TDP brains acted as a seed of TDP-43 aggregation when it was introduced in SH-SY5Y cells, and that TDP-43 aggregation was transmitted to other co-cultured cells. In addition, Feiler *et al.* (2015) confirmed a trans-synaptic cell-to-cell transmission of TDP-43 oligomer using a novel TDP-43-oligomer quantification system. These reports suggest that TDP-43 aggregation can be transmitted from cell to cell and it may explain the disease spreading in ALS. Many lines of evidence suggest that exosomes can contribute to propagation of pathological proteins in some neurodegenerative diseases (Fevrier *et al.*, 2004; Rajendran *et al.*, 2006; Asai *et al.*, 2015). Whether exosomes play a role in propagation of TDP-43 is not fully resolved. TDP-43 has been detected in exosome fractions from cultured cells (Nonaka *et al.*, 2013; Feiler *et al.*, 2015) and from human CSF (Feneberg *et al.*, 2014; Ding *et al.*, 2015). However, it remains unclear whether exosomal TDP-43 secretion is increased in ALS/FTLD disease, which cell types secrete TDP-43 and what is the role of exosome secretion in pathogenesis.

Here, we report that secretion of TDP-43 can occur via exosomes in neuronal cells, primary neurons or human brains. We show that exosomal TDP-43 secretion is increased under pathological conditions that promote its aggregation and that exosomes containing pathological TDP-43 may play a key role in the propagation of TDP-43 proteinopathy. However, pharmacological inhibition of exosome secretion in transgenic mice expressing human TDP-43$^{A315T}$ mutant exacerbated neuronal aggregation of TDP-43 and disease phenotypes. Therefore, therapeutic strategies for ALS based on inhibition of exosome production would seem inappropriate as our *in vivo* data suggest that exosome secretion plays an overall beneficial role in the neuronal clearance of pathological TDP-43.

# Materials and methods

## Human brain samples

The use of the human tissue samples described in this article was performed in accordance to the Committee on Research Ethics of Institut universitaire en santé mentale de Quebec (IUSMQ).

## Animals and GW4869 administration

The transgenic mice bearing a human genomic fragment encoding TDP-43$^{A315T}$ are reported previously (Swarup *et al.*, 2011). The TDP-43$^{A315T}$ mice used here did not develop behavioural and pathological changes as severe as those described previously (Swarup *et al.*, 2011). The attenuated phenotypes were likely due to a reduction in expression levels of TDP-43$^{A315T}$ transgene in this mouse line. The TDP-43$^{A315T}$ mice in our study exhibited a 1.2- to 1.4-fold overexpression of TDP-43 expression (Supplementary Fig. 1) in contrast to a 3-fold increase in the original mouse line described before (Swarup *et al.*, 2011). GW4869 {N,N0-Bis[4-(4,5-dihydro-1H-imidazol-2-yl)phenyl]-3,30-p-phenylene-bis-acrylamide dihydrochloride} powder (Cayman Chemical) was reported to reduce neutral sphingomyelinase activity in mouse cortices by intraperitoneal injection (Tabatadze *et al.*, 2010). We used this compound to inhibit exosome secretion in mouse CNS. GW4869 was dissolved in dimethyl sulphoxide (DMSO) at 8 mg/ml and stored at −20°C. The working solution was prepared in 0.9% normal saline freshly before use with a final concentration of 0.3 mg/ml. Twenty-week-old mice were injected intraperitoneally with 200 μl of GW4869 solution (60 μg per mouse) or 200 μl of 3.75% DMSO saline twice a week until 42 weeks of age. The use and maintenance of the mice described in this article was performed in accordance to the Guide of Care and Use of Experimental Animals of the Canadian Council on Animal Care.

## Rotarod analysis

Motor performance of the mice was analysed every 2 weeks with an accelerated rotarod, starting at 4 rpm for female or 3 rpm for male mice with 0.2 rpm/s acceleration, and time was noted when the mice fell off the roll. Three trials were done per animal, and the best score was calculated for statistics and graphs.

## Novel object recognition test

Novel object recognition test was done at the end of the animal analysis at 42 weeks of age. On the first day, the mice were placed in the box (width: 40 cm, depth 40 cm, height: 35 cm) for 5 min for habituation. On the second day, two identical objects were put in the box, and the time spent exploring each object was recorded during 5 min of the observation. On the third day, the one object was replaced to a different object, and the analysis was done as the day before. The data of both genders were put together for this analysis.

## DNA constructs

The V5-tagged wild-type (WT) and 25 kDa C-terminal fragment (25CTF) of human TDP-43 (hTDP-43) plasmids were described before (Iguchi *et al.*, 2012; Takagi *et al.*, 2013). For disease mutants, A315T or G348C of hTDP-43 vectors, primers containing the mutant substitutions were used to mutagenize wild-type-hTDP-43 (KOD-Plus-Mutagenesis kit; Toyobo). The sequences of all constructs were verified using

CEQ 8000 genetic analysis system (Beckman Coulter). TSG101-Cherry vector (Lee *et al.*, 2008) was purchased from Addgene.

## Cell culture and treatment

Mouse neuroblastoma Neuro2a and human embryonic kidney 293 (HEK293) cells were cultured in a humidified atmosphere of 95% air/5% $CO_2$ in a 37°C incubator in Dulbecco's modified Eagle's medium (DMEM) supplemented with 10% foetal bovine serum (FBS) and 1% sodium pyruvate. The transfections of the intended plasmids were performed using Lipofectamine® 2000 (Invitrogen), according to the manufacturer's instructions. Co-transfection with wild-type-hTDP-43 plasmid and small interfering (si)RNA was done with jetPRIME (Polyplus transfection), according to the manufacturer's instructions. siRNAs against *Rab27a* and control RNA were purchased from Dharmacon. The target sequences of *Rab27a* were CUGUUAUGUAGAACGCUGA (Oligo1) and GCUGCAGCUUUGUAUGAUU (Oligo2). Twenty-four hours after transfection, the medium was replaced with DMEM plus 10% exosome-depleted FBS, 1% sodium pyruvate, and 5 mM N6,2′-O-dibutyryl cAMP (dbcAMP, Sigma-Aldrich), which was added to differentiate Neuro2a cells. The cells were cultured for 24 h. For the interventions, bafilomycin A1, rapamycin, MG132, ethacrinic acid (Sigma-Aldrich), or GW4869 were added in the exosome-depleted medium.

## Primary astrocytes, microglia and cortical neurons

For cultures of primary neurons, the cerebrum was taken from embryonic Day 15 embryos of Bl/C57 mice, and incubated in phosphate-buffered saline (PBS) with 0.25% trypsin at 37°C for 30 min. Digested tissue was picked up with < 1 ml of trypsin solution. The solution was filled up to 3 ml with Opti-MEM™ containing 10% FBS, triturated gently, and incubated with DNase (0.1 K/ml) at 37°C for 5 min. Cell suspensions were centrifuged at 300 g for 10 min, and the pellet was diluted by 10 ml Opti-MEM™ with 10% FBS. Cortical cells from one embryo were plated on a poly-L-lysine-coated 10 cm dish. After 1 h the medium was exchanged to Neurobasal® medium containing B27 supplement, Antibiotic-Antimycotic, and GlutaMAX™ (Thermo Fissure Scientific). After 3 days, a half of the medium was exchanged, and after another 3 days, the medium was harvested for the exosome purification.

For primary astrocyte and microglial cell cultures, the cortex of postnatal Day 1 Bl/C57 mice was dissociated using the same protocol as for the primary cortical neurons. Cortical cells from two mice were plated on a T75 flask with DMEM-F12 with 10% FBS. The medium was replaced to the new medium but with 5 ng/ml granulocyte-colony stimulating factor (G-CSF) every 3 days until it became confluent. The flask of confluent mix glial cells was shaken for 6 h at 200 rpm, and the medium was replaced with a fresh culture medium. The floating microglial cells were recovered by centrifugation at 300 g for 10 min. The remaining microglial cells were separated from astrocytes by mild trypsinization protocol (Saura *et al.*, 2003). Trypsinized astrocytes were transferred into a new T75 flask. Previously collected microglial cells were added in the flask of remaining microglial cultures. After 3 days, the medium of primary astrocytes or microglial cells was replaced with the exosome-depleted medium, and after another 3 days it was harvested for exosome purification. Lipopolysaccharide (LPS, Sigma Aldrich) was added in the medium 24 h before the purification.

## Purification of exosomes

FBS was centrifuged at 100 000 g for 16 h at 4°C to remove exosomes, and the supernatant was carefully collected and added into DMEM or DMEM/F12. DMEM or DMEM/F12 with 10% exosome-depleted FBS and 1% sodium pyruvate was used for the cell culture before the exosome purification.

A culture media of Neuro2a cells, primary cortical neurons, astrocytes, or microglial cells was harvested and spun at 300 g for 10 min to remove cells. The supernatants were sequentially centrifuged at 2000 g for 10 min, 20 000 g for 30 min, and 100 000 g for 60 min. The final pellet (P100) was resuspended with 3% sodium dodecyl sulphate (SDS) sample buffer for whole extract analysis or RIPA buffer for RIPA-soluble/-insoluble extraction. The whole volume of the lysate was loaded onto the gels for immunoblots. Although this pellet is exosome-enriched fraction, sucrose density gradient centrifugation (0.25–2.5 M) was done for the further confirmation. The P100 pellet was resuspended with 2 ml of 2.5 M sucrose/PBS solution, and a step gradient of sucrose solution (2.25, 2.0, 1.75, 1.5, 1.25, 1.0, 0.75, 0.5, and 0.25 M; 1 ml of each) was layered over the 2.5 M sucrose solution. The gradient solution was centrifuged at 200 000 g for 15 h. From the top of the gradient, 0.8 ml of fractions were collected. Each fraction was diluted with 10 ml of PBS and centrifuged at 100 000 g for 1 h. Each pellet was resuspended with 3% SDS sample buffer. The whole volume of lysate was loaded on gels for immunoblots. All of the procedures were done at 4°C.

The purification of brain exosomes was done as described before (Perez-Gonzalez *et al.*, 2012) with minor modifications. Briefly, 200 µg of human frozen brain or a half of frozen mouse brain was dissected and incubated with 20 units/ml papain (Worthington) in 3 ml of Hibernate® E solution (BrainBits) for 15 min at 37°C. The brain tissue was gently homogenized by pipetting in 6 ml of Hibernate® E solution and sequentially filtered through 70 µm mesh filter and 0.2 µm syringe filter. The homogenate was sequentially centrifuged at 300 g for 10 min, 2000 g for 10 min, and 20 000 g for 30 min at 4°C. The supernatant was pelleted by centrifugation at 100 000 g for 60 min at 4°C. The pellet was fractionated with sucrose density gradient centrifugation as described above. Then, the gradient solution was separated into six fractions (1, 2, 2, 2, 2, and 3 ml from the top). The pellet of each fraction was diluted with 10 ml of PBS and centrifuged at 100 000 g for 60 min at 4°C. The final pellet was diluted with 50 µl of PBS, and 15 µl of each fraction was used for immunoblots. As shown in Supplementary Fig. 5, an exosome marker, flotillin 1, was predominantly detected in the second and third fractions. Then we put the whole solution of the second and the third fractions together in the ultracentrifuge tube, and diluted with 10 ml of PBS, followed by centrifugation at 100 000 g for 60 min at 4°C. The pellet was resuspended with 50 µl of PBS, and 5 µl of the solution was lysed with 10 µl of RIPA buffer and centrifuged at 20 000 g for 15 min at 4°C. The supernatant was kept for RIPA soluble fraction, and the pellet was lysed with 15 µl of 3% SDS sample buffer. The whole amount of RIPA-soluble or -insoluble lysate was loaded onto

gels for immunoblots. A 10-µl sample of the third fraction was taken for electron microscopy.

For exosome purification from mouse serum, 100 µl of serum was purified from 250 µl of blood and diluted with 10 ml of PBS, and then followed the same procedure for exosome purification of cultured cells as described above.

## Exosome induction treatment

Neuro2a cells were cultured in six wells of a 24-well cell culture plate and transfected with V5-hTDP-43 the day before. Human brain exosomes were purified as shown above. Each 10-µg of exosomes purified from control (Control-2, 3 or 4) or ALS (ALS-1, 3 or 5) brains were labelled with PKH67 Green Fluorescent Cell Linker Kit (Sigma-Aldrich). Briefly, 2 µl of dye solution was diluted with 100 µl of dilutant C solution, and centrifuged at 15 000*g* for 10 min at 20°C to remove aggregated dye. The supernatant was mixed with 100 µl of dilutant C containing the exosomes, and incubated for 5 min. The mixture was diluted with 1 ml of exosome-depleted FBS, incubated for 5 min, and diluted with 8 ml of PBS. The solution was centrifuged at 100 000*g* for 1 h at 20°C, and the pellet was washed with 10 ml of PBS and centrifuged again at 100 000*g* for 1 h at 20°C. The pellet was resuspended with 500 µl of exosome-depleted culture medium, and filtered with 0.2-µm syringe filter. Finally, the culture medium of Neuro2a cells was replaced with the medium containing PKH-67-labelled exosomes. After 24 h immunocytochemistry was done with V5 antibody. The stained cells were imaged with FV1000 laser confocal microscope (Olympus), and rate of cells with cytoplasmic TDP-43 in cells internalizing PKH67-exosomes was analysed. More than 100 cells with PKH67-exosomes were evaluated for each well.

## Western blot analysis

Neuro2a cells or mouse tissues were lysed with RIPA buffer (50 mM 1M Tris pH7.4, 150 mM NaCl, 1% Triton X-100, 1% deoxycholate, 0.1% SDS) using downs homogenizer for mouse tissue, sonicated, and centrifuged at 20 000*g* for 15 min at 4°C. The supernatant was kept for RIPA soluble fraction, and the pellet was resuspended with RIPA buffer again for washing, and centrifuged at 20 000*g* for 15 min. The final pellet was lysed with 3% SDS sample buffer. Twenty micrograms of protein was loaded and separated by SDS-PAGE. Primary antibodies are listed in Supplementary Table 1.

## Electron microscopy

Electron microscopy was performed as described previously (Lasser *et al.*, 2012) with some modifications. Briefly, vesicles were applied to a Formvar®-coated copper or nickel grid, and fixed with 4% paraformaldehyde in PBS; immunostained with primary antibodies listed in Supplementary Table 1, followed by 10 nm gold-labelled mouse or rabbit secondary antibody (Electron Microscopy Science). Samples were post-fixed with 2.5% glutaraldehyde, contrasted with 2% uranyl acetate, and embedded with 0.13% methylcellulose and 0.4% uranyl acetate. Grids were examined with a Tecnai12 transmission electron microscope (100 kV; Philips Electronic) equipped with an integrated Mega-View II digital camera (SIS).

## Immunofluorescence

For immunocytochemistry Neuro2a cells were fixed with 4% paraformaldehyde (PFA) buffer for 30 min, and incubated with 1% Triton™ X-100/PBS for 5 min. Then washed cells were blocked with 2% BSA/PBS buffer for 30 min, and incubated with primary antibodies listed in Supplementary Table 1. Mice were perfused with 4% PFA buffer, and post-fixed for 3 h in 4% PFA. We then cut 25-µm thick tissue sections by microtome and dehydrated them on slide glass. The sections were first microwaved for 5 min in 50 mM citrate buffer (pH 6.0) with 0.05% Tween-20, treated with 2% BSA blocking buffer, and incubated overnight at 4°C with primary antibodies listed in Supplementary Table 1. After washing, sections were incubated with the indicated secondary antibody for 30 min, mounted with ProLong® gold antifade reagent (Thermo Fissure Scientific), and then imaged with FV1000 laser confocal microscope.

## Analysis of neuromuscular junction and muscle

Muscles were quickly frozen by liquid nitrogen, and cut by cryostat. The fixation was done with 1:1 methanol and acetone mixture. For analysis of neuromuscular junction, 20-µm thick frozen longitudinal sections of the tibialis anterior muscle were incubated overnight with anti- SMI31 and SV-2 antibody. After washing, sections were incubated with goat anti-rabbit and anti-mouse IgG conjugated with Alexa 488 (1:500 for each, Invitrogen) and tetramethylrhodamine α-bungarotoxin (1:500, Invitrogen) for 30 min and mounted with ProLong® gold (Invitrogen). More than 100 neuromuscular junctions from each mouse were analysed (*n* = 3 mice for each group). To evaluate muscle atrophy, 10-µm thick transverse sections of gastrocnemius muscles were stained with laminin antibody. More than 100 muscle fibre sizes were measured for each mouse by ImageJ software (Schneider *et al.*, 2012). Overall 18 mice were analysed for neuromuscular junction and muscle fibre size. Three mice (two males and one female) were analysed for each wild-type mouse group and six mice (three males and three females) were analysed for each TDP-43[A315T] mouse group.

## Statistical analyses

Statistical differences were analysed by ANOVA and Bonferroni *post hoc* analyses for multiple group comparisons and the unpaired Student's *t*-test for two group comparisons (SPSS version 15.0, SPSS Inc.).

# Results

## TDP-43 is secreted via exosomes in Neuro2a cells

To determine if TDP-43 is secreted via exosomes, exosomes were purified from the cultured media of Neuron2a cells by sequential centrifugations. Electron microscopy revealed that the fraction of final pellet (P100) was a relatively
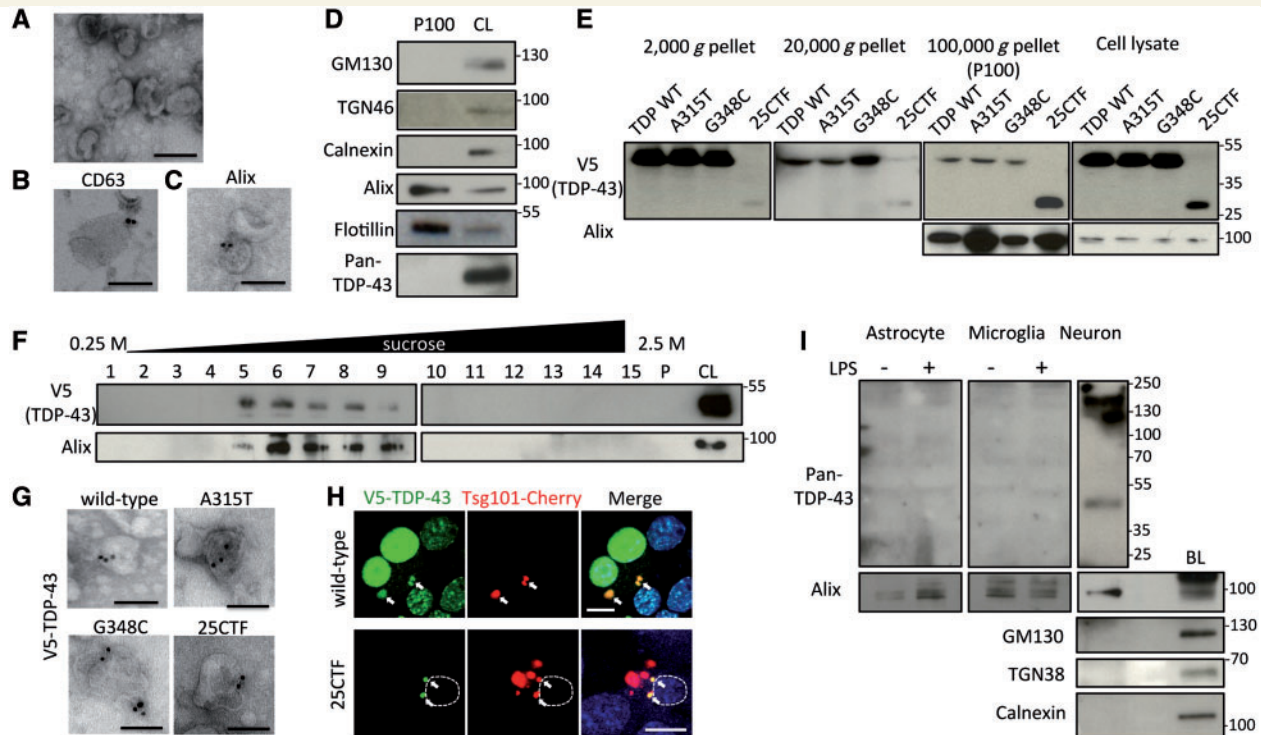
**Figure 1 TDP-43 is secreted via exosomes in Neuro2a cells.** (**A**) Electron microscopic image of secreted vesicles from Neuro2a cells. Scale bar = 100 nm. (**B** and **C**) Immunoelectron microscopic images with anti-CD63 (**B**) or Alix (**C**) antibodies. Scale bars = 100 nm. (**D**) Immunoblots of P100 and cell lysate (CL) of Neuro2a cells. (**E**) Immunoblots of pellets from different centrifugations of medium or cell lysates of Neuro2a cells transfected with wild-type (WT), A315T, G348C, or C-terminal fragment (25CTF) of hTDP-43. (**F**) Sucrose density gradient fractionation of P100 of Neuro2a cells transfected with V5-hTDP-43. Fifteen fractions of sucrose gradient, pellet (P), and cell lysate of Neuro2a cells. (**G**) Immunoelectron microscopic image of P100 of Neuro2a cells transfected with wild-type, A315T, G348C, or 25CTF hTDP-43 with V5 antibody. Scale bars = 100 nm. (**H**) Immunofluorescent images of Neuro2a cells transfected with V5-wild-type or -25CTF hTDP-43, Tsg101-Cherry (green; V5-TDP-43, red; Tsg101-Cherry, blue; DAPI). Dotted line indicates boundary of nucleus. Scale bars = 10 μm. Arrows indicate co-localization of V5-TDP-43 and Tsg101-Cherry. (**I**) Immunoblots of exosome fraction from primary astrocytes, primary microglial cells or primary neurons with brain lysate (BL) of C57BL6 mouse. Primary astrocytes or microglial cells were treated with DMSO or LPS (100 ng/ml) for 24 h.

homogenous population of 50 to 100 nm diameter cup-shaped vesicles (Fig. 1A), which have typical exosome morphologies. In addition, these vesicles were immunopositive for the exosome markers CD63 and Alix (Fig. 1B and C). Immunoblots revealed that this fraction was negative for GM130, TGN38, or Calnexin, which are cis-, trans-Golgi, or endoplasmic reticulum markers, respectively, whereas it was positive for the exosome markers Alix and flotillin-1 (Fig. 1D). However, TDP-43 was not detected in this fraction (Fig. 1D). Then, we prepared exosomes from media of Neuro2a cells transfected with expression vectors encoding various human TDP-43 (hTDP-43) species including V5-tagged wild-type, two disease mutants, A315T and G348C, and 25 kDa C-terminal fragment (25CTF) of hTDP-43. Remarkably, each exogenous TDP-43 species was detected in P100 exosome fraction from transfected Neuro2a cells (Fig. 1E). The amount of 25CTF hTDP-43 in P100 was larger than wild-type hTDP-43 whereas there was no obvious difference between two disease mutants and wild-type hTDP-43. For further confirmation, P100 of wild-type hTDP-43-transfected cells was

fractionated by sucrose gradient centrifugation. TDP-43 was detected between the third and seventh fractions together with the exosome-marker Alix (Fig. 1F). Furthermore, immunoelectron microscopy with V5 antibody showed that each TDP-43 species (wild-type, A315T, G348C or 25CTF of hTDP-43) could be detected in exosomes after vector transfection in Neuro2a cells (Fig. 1G). These data suggest that TDP-43 can be secreted via exosomes when it is overexpressed. As exosomes originate from late endosomes/multivesicular bodies (MVBs), we examined the co-localization of TDP-43 and Tsg101, which is a marker of endosome. The immunofluorescent analyses showed that wild-type or 25CTF of hTDP-43 were co-localized with Tsg101 in Neuro2a cells (Fig. 1H), suggesting that TDP-43 is processed by endosomal sorting machinery.

In addition, we purified exosomes from primary astrocytes, microglial cells, or cortical neurons of C57BL6 mice to determine which cell types secrete TDP-43 via exosomes in the CNS. TDP-43 was detected in exosome fraction from primary cortical neurons (Fig. 1I) but it was not

detected in exosome fraction from primary astrocytes or microglial cells even after LPS stimulation.

## Autophagy, proteasome and protein aggregation are modulators of TDP-43 exosomal secretion

Late endosomes/MVBs are at the origin of exosomes but they can also fuse with autophagosomes or lysosomes with an involvement in lysosomal degradation pathway. To investigate the effect of autophagy modulation on exosomal secretion of TDP-43, Neuro2a cells expressing hTDP-43 were treated with bafilomycin A1, an autophagy inhibitor or with rapamycin, an inducer. Neither treatment changed the proportion of soluble and insoluble TDP-43 (Fig. 2A and B) or caused TDP-43 aggregation (Fig. 2C). However, exosomal TDP-43 was significantly increased by bafilomycin A1 treatment (Fig. 2D and E). The levels of exosomal marker Alix were reduced by rapamycin treatment reflecting an inhibition of exosome secretion in the media of Neuro2a cells (Fig. 2D and E). As a consequence of this treatment, there was a slight decrease of exosomal TDP-43 albeit it was not statistically significant.

We next treated Neuro2a cells expressing hTDP-43 with a proteasome inhibitor, MG132. MG132 (1 μM) increased insoluble TDP-43 (Fig. 2F and G) and phosphorylated cytoplasmic aggregates of TDP-43 (Fig. 2H). Soluble TDP-43 was not decreased by MG132 as the mirror of increase of insoluble TDP-43. As proteasome inhibitor halts degradation of proteins, the total amount of TDP-43 is supposed to be increased. Actually, immunoblots of the whole cell lysate with SDS sample buffer showed an increase of total amount of TDP-43 by MG132 treatment (Supplementary Fig. 2). Exosomal TDP-43 secretion was significantly increased by this treatment (Fig. 2I and J). A certain amount of exosomal TDP-43 induced by bafilomycin and MG132 were insoluble (Fig. 2K). In addition, an oxidative stress inducer, ethacrynic acid, reduced soluble TDP-43 and increased insoluble TDP-43 in a dose-dependent manner (Fig. 2L and M) and induced phosphorylated intra-nuclear and cytoplasmic aggregations in the cell treated with ethacrynic acid (Fig. 2N), as reported before (Iguchi *et al.*, 2012). Immunoblots of exosomal fractions revealed that ethacrynic acid treatment increased exosomal insoluble TDP-43 secretion in a dose-dependent fashion (Fig. 2O and P).

We assessed by reverse transcriptase-quantitative polymerase chain reaction (RT-qPCR) the levels of human *TARDBP* mRNA and of endogenous *Tardbp* mRNA in TDP-43-transfected or non-transfected Neuro-2a cells (Supplementary Fig. 3). It should be noted that our human TDP-43 plasmid vector did not contain the 3'UTR region of *TARDBP* mRNA, which is involved in the autoregulation mechanism. As expected, there was a slight decrease of mouse endogenous *Tardbp* mRNA in cells transfected with human TDP-43 plasmid vector.

Conditions promoting exosome secretion had different effects on the human and mouse TDP-43 mRNAs. Thus, MG132 treatment increased human *TARDBP* mRNA level whereas mouse endogenous *Tardbp* mRNA remained unchanged. On the other hand, bafilomycin treatment decreased mouse *Tardbp* mRNA level whereas human *TARDBP* mRNA level remained unchanged. Inhibition of exosome secretion by GW4869 treatment did not affect the levels of either mouse or human *TARDBP* mRNAs.

## Exosomal TDP-43 secretion is increased in human amyotrophic lateral sclerosis brain

To validate the physiological relevance of the phenomenon, we decided to prepare exosomes from frozen postmortem temporal cortices of patients with sporadic ALS and disease control subjects (Supplementary Table 2). Before exosome preparation, we performed immunoblot of salkosyl-insoluble fractions of the cortices to check if these regions were affected. Three of six ALS samples were positive for phosphorylated TDP-43 (Supplementary Fig. 4), indicating that these three temporal cortices have TDP-43 pathology. Phosphorylation at Ser409/410 of TDP-43 has been identified as a disease-specific modification of ALS and FTLD-TDP (Hasegawa *et al.*, 2008). Exosomes were prepared from the brain of these three ALS patients and of controls. Following sucrose density gradient centrifugation, TDP-43 species were detected mainly in the second and third fractions together with the exosome marker flotillin-1 in all of the subjects (Supplementary Fig. 5), and the amount of that TDP-43 from ALS patients was higher than that from control brains. We then pooled the second and third fraction of each subject and loaded together. The immunoblot with pan-TDP-43 polyclonal antibody showed multiple bands between 15 and 70 kDa (Fig. 3A), and densitometric analysis normalized with flotillin-1 revealed the total exosomal levels of TDP-43 in ALS were significantly increased compared with control samples (Fig. 3B). The anti-TDP-43 C-terminal antibody detected 15 and 28 kDa bands at extremely higher levels in exosomes from ALS than from controls (Fig. 3C). These TDP-43 species were not phosphorylated at Ser409/410 (Supplementary Fig. 6). Immunoblots of the second and third fractions from Control patient 1 were compared with immunoblots from HEK293 total cell lysate. These fractions from Control patient 1 were negative for cis-, trans-Golgi, or endoplasmic reticulum marker, but positive for both exosome markers, flotillin-1 and CD63 (Fig. 3D). Electron microscopy of these fractions from Patient ALS-2 revealed mainly 50 to 100 nm diameter cup-shaped exosome-like structures (Fig. 3E), which were immuno-positive for the exosome marker Tsg101 (Fig. 3F) and for TDP-43 (Fig. 3G). These data suggest that this fraction is a pure
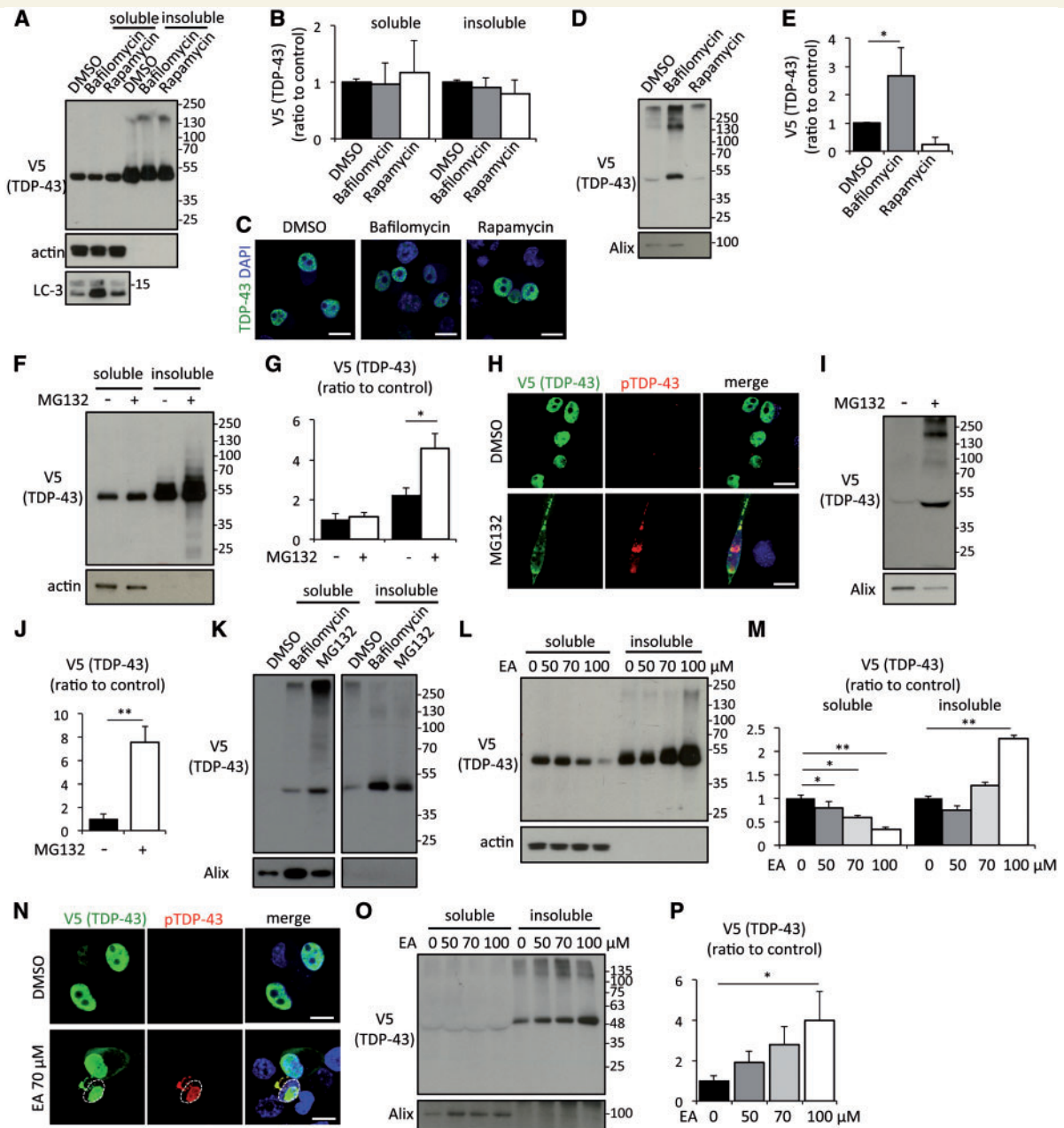
**Figure 2** **Autophagy, proteasome and protein aggregation are modulators of TDP-43 exosomal secretion.** (**A**) Immunoblots of RIPA-soluble or -insoluble fraction of Neuro2a cells treated with DMSO, 100 nM of bafilomycin A1 or 0.4 µM of rapamycin for 24 h. Neuro2a cells were transfected with V5-hTDP-43. (**B**) Densitometric quantification of V5 ($n = 3$ for each group). Error bars indicate standard deviation (SD). (**C**) Immunofluorescent images of Neuro2a cells treated with DMSO, bafilomycin A1, or rapamycin (green; V5-TDP-43, blue; DAPI). Scale bars = 10 µm. (**D**) Immunoblots of exosome fraction of Neuro2a cells. (**E**) Densitometric quantification of V5 ($n = 3$ for each group, $*P < 0.05$, ANOVA followed by Bonferroni *post hoc* tests). Error bars indicate SD. (**F**) Immunoblots of RIPA-soluble or -insoluble fraction of Neuro2a cells treated with DMSO or 1 µM MG132 for 24 h. Neuro2a cells were transfected with V5-hTDP-43. (**G**) Densitometric quantification of V5 ($n = 3$ for each group). Error bars indicate SD. (**H**) Immunofluorescent images of Neuro2a cells treated with DMSO or MG132 (green; V5-TDP-43, red; phosphoTDP-43 Ser409/410, blue; DAPI). Scale bars = 10 µm. (**I**) Immunoblots of exosome fraction of Neuro2a cells. (**J**) Densitometric quantification of V5 ($n = 3$ for each group, $*P < 0.05$, ANOVA followed by Bonferroni *post hoc* tests). Error bars indicate SD. RIPA-soluble or -insoluble exosome fraction of Neuro2a cells treated with DMSO or 100 nM bafilomycin A1. (**K**) Immunoblots of RIPA-soluble or -insoluble exosome fractions of Neuro2a cells treated with DMSO, bafilomycin, or MG132. (**L**) Immunoblots of RIPA-soluble or -insoluble fractions of Neuro2a cells treated with ethacrynic acid (EA) for 24 h. Neuro2a cells were transfected with V5-hTDP-43. (**M**) Densitometric quantification of V5 ($n = 3$ for each group, $*P < 0.05$, and $**P < 0.01$, ANOVA followed by Bonferroni *post hoc* tests). (**N**) Immunofluorescent images of Neuro2a cells treated with DMSO or 70 µM ethacrynic acid (green; V5-TDP-43, red; phosphoTDP-43 Ser409/410, blue; DAPI). Dotted line indicates boundary of nucleus. Scale bars = 10 µm. (**O**) Immunoblots of RIPA soluble or insoluble exosome fractions of Neuro2a cells treated with ethacrynic acid. (**P**) Densitometric quantification of V5 ($n = 3$ for each group, $*P < 0.05$, ANOVA followed by Bonferroni *post hoc* tests).
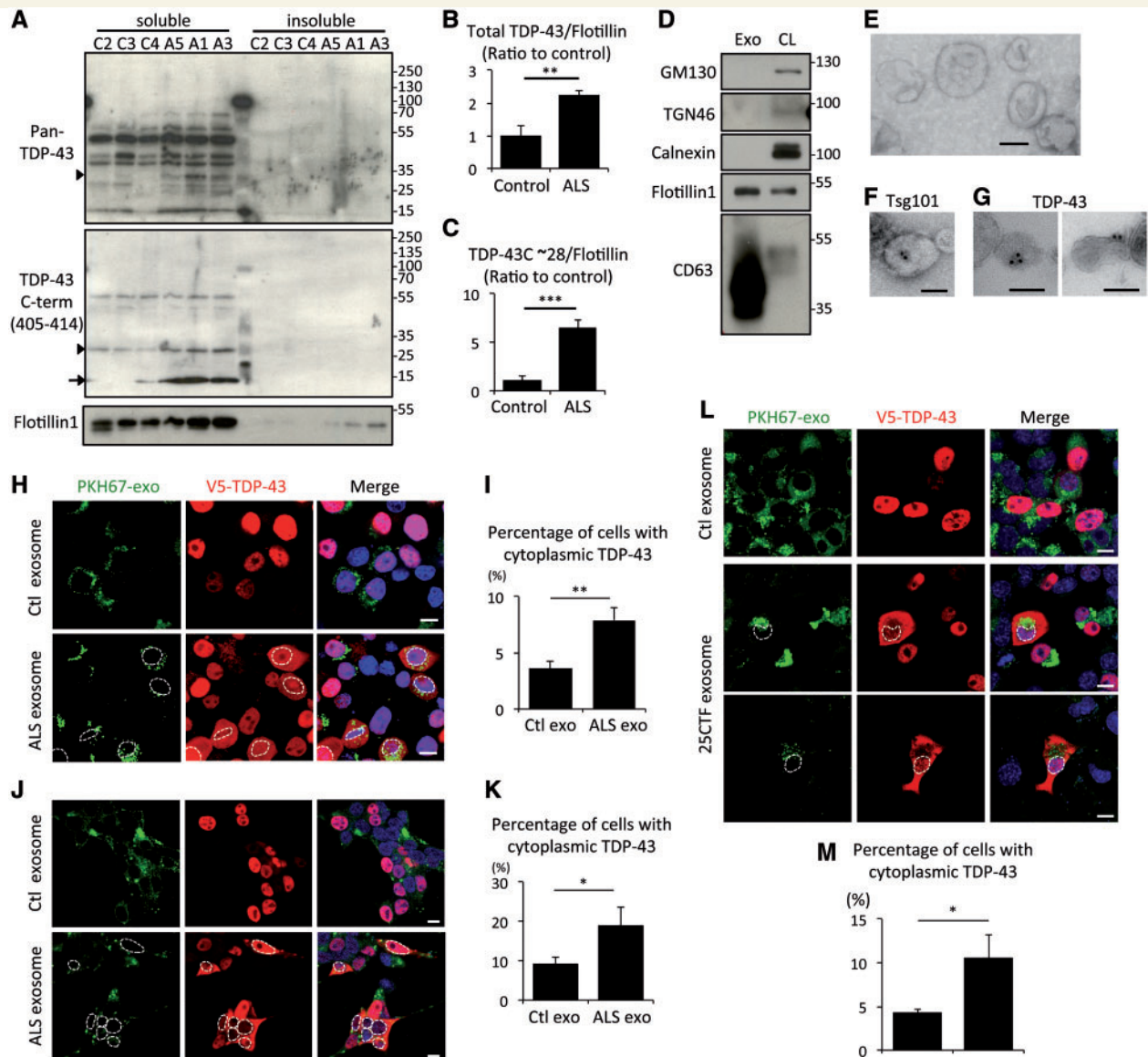
**Figure 3 Exosomal TDP-43 is increased in ALS brain.** (**A**) Immunoblots of exosomal fraction from control and ALS brains using anti-pan-TDP-43 or anti-TDP-43 C-term (405-414) antibody. Arrowhead and arrow indicate 28 kDa and 15 kDa of TDP-43 C-terminal fragment, respectively. (**B** and **C**) Densitometric quantification of total TDP-43 from pan-TDP-43 blot (**B**) or of TDP-43 C-terminal fragment ($\sim$28 kDa) (**C**) normalized with flotillin-1 ($n = 3$ for each group, **$P < 0.01$, and ***$P < 0.001$, unpaired Student's $t$-test). Error bars indicate SD. (**D**) Immunoblots of exosome fraction from Control patient 1 brain and cell lysate (CL) of HEK293 cells. (**E–G**) Electron microscopic images of exosome fraction of Patient ALS-3 brain. The vesicles were positive for Tsg101 (**F**) or TDP-43 (**G**). Scale bars = 100 nm. (**H**) Fluorescent images of Neuro2a cells treated with PKH67-labeled exosomes (green: PKH67, red; V5-TDP-43, blue; DAPI) from control or ALS brain. Neuro2a cells were transfected with V5-hTDP-43. Scale bars = 10 μm. (**I**) Percentage of cells with cytoplasmic TDP-43 redistribution in cells internalizing PKH67-labelled exosomes ($n = 3$ for each group, *$P < 0.05$, unpaired Student's $t$-test). Neuro2a cells were treated with each 10 -μg exosomes purified from three different control (Control patients 2, 3 and 4) or ALS (Patients ALS-1, 3 and 5) brains for 24 h. More than 100 cells were evaluated for each. (**J**) Fluorescent images of HEK293 cells treated with PKH67-labelled exosomes (green: PKH67, red; V5-TDP-43, blue; DAPI) from control or ALS brains. Cells were transfected with V5-hTDP-43. Scale bars = 10 μm. Dotted lines indicate boundary of nucleus. (**K**) Percentage of cells with cytoplasmic TDP-43 redistribution in cells internalizing PKH67-labelled exosomes ($n = 3$ for each group, *$P < 0.05$, unpaired Student's $t$-test). HEK293 cells were treated with each 10 μg exosomes purified from three different controls (Control 2, 3 and 4) or ALS (Patients ALS-1, 3 and 5) brains for 24 h. More than 100 cells were evaluated for each. (**L**) Fluorescent images of Neuro2a cells treated with PKH67-labelled exosomes (green: PKH67, red; V5-TDP-43, blue; DAPI) from control or ALS brain. Cells were transfected with V5-hTDP-43. Scale bars = 10 μm. Dotted lines indicate boundary of nucleus. (**M**) Percentage of cells with cytoplasmic TDP-43 redistribution in cells internalizing PKH67-labelled exosomes ($n = 3$ for each group, *$P < 0.05$, unpaired Student's $t$-test). Neuro2a cells were treated with exosomes purified from Neuro2a cells transfected with mock or TDP-43 C-terminal fragment plasmid (25CTF) for 24 h. More than 100 cells were evaluated for each plate.
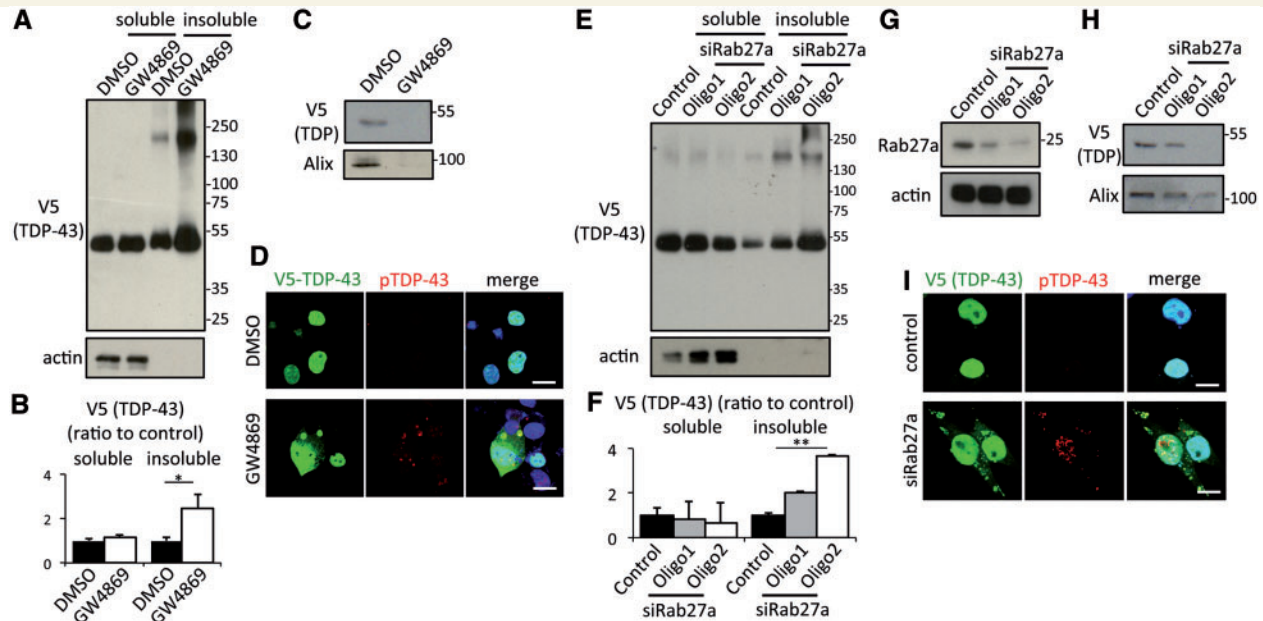
**Figure 4 Inhibition of exosome secretion induces TDP-43 aggregation in Neuro2a cells.** (**A**) Immunoblots of RIPA-soluble or -insoluble cell lysate of Neuro2a cells treated with DMSO or 10 μM GW4869 for 24 h. Neuro2a cells were transfected with V5-hTDP-43. (**B**) Densitometric quantification of V5 (n = 3 for each group, **P < 0.01, unpaired Student's t-test). Error bars indicate SD. (**C**) Immunoblots of exosome fraction from Neuro2a cells treated with DMSO or 10 μM GW4869. (**D**) Immunofluorescent image of Neuro2a cells (green; V5-TDP-43, red; phosphoTDP-43 ser409/410, blue; DAPI). Scale bars = 10 μm. (**E**) Immunoblots of cell lysate of Neuro2a cells transfected with V5-TDP-43 and *Rab27a* siRNA. (**F**) Immunoblots of exosome fraction from Neuro2a cells transfected with V5-TDP-43 and *Rab27a* siRNA. (**G**) Immunoblots of RIPA-soluble or -insoluble fraction in Neuro2a cells transfected with V5-TDP-43 and *Rab27a* siRNA. (**H**) Densitometric quantification of V5 (n = 3 for each group, **P < 0.01, ANOVA followed by Bonferroni *post hoc* tests). Error bars indicate SD. (**I**) Immunofluorescent analysis of Neuro2a (green; V5-TDP-43, red; phosphoTDP-43 Ser409/410, blue; DAPI). Scale bars = 10 μm.

exosome fraction and that TDP-43 is secreted together with exosomes in human brain and at higher levels in ALS brain.

To examine whether ALS exosomes might act as a seed for TDP-43 aggregation, we added ALS or control brain exosomes labelled with PKH67 to the medium of cultured Neuro2a cells for a period of 24 h. These exosomes were well internalized by Neuro2a cells and a certain number of cells internalized with ALS exosomes showed cytoplasmic TDP-43 redistribution (Fig. 3H). Although few cells exposed to control exosomes also exhibited such TDP-43 redistribution, it was at much lower extent than the cells exposed to ALS exosomes (Fig. 3I). The same experiment was done with HEK293 cells. ALS exosomes induced TDP-43 cytoplasmic redistribution in HEK cells as well (Fig. 3J and K). In addition, we treated Neuro2a cells with exosomes from Neuro2a cells transfected with TDP-43 25CTF, and observed significantly more TDP-43 cytoplasmic redistributions in the cell internalized 25CTF-containing exosomes than in the cells with control exosomes (Fig. 3L and M). Moreover, we treated primary cortical neurons of TDP-43[G348C] mouse with TDP-43 25CTF-containing exosomes, but there was no obvious TDP-43 cytoplasmic redistribution in the neurons, although those exosomes were internalized (Supplementary Fig. 7).

# Exosome secretion is a key pathway for the clearance of aggregated TDP-43

According to the data of Neuro2 cells treated with autophagy modulators, proteasome inhibitor and ethacrinic acid, exosome secretion might play a buffering role of TDP-43 aggregate. This raises a concern about whether inhibition of exosome secretion may induce TDP-43 aggregate. We inhibited exosome secretion in Neuro2a cells with two different approaches. First, we focused on the neutral sphingomyelinase 2 (nSMase2), which converts sphingomyelin to ceramide and which has been reported to mediate exosome secretion in neurons, astrocytes or microglial cells (Dinkins *et al.*, 2014; Asai *et al.*, 2015). An inhibitor of nSMase2, GW4869, was found to reduce exosome secretion in Neuro2a cells in a dose-dependent manner (Supplementary Fig. 8). Therefore, we treated Neuro2a cells overexpressing hTDP-43 with GW4869. This compound reduced exosomal TDP-43 secretion (Fig. 4C) and it significantly increased insoluble TDP-43 in Neuro2a cells (Fig. 4A and B). In addition, immunocytochemistry revealed that GW4869 treatment induced formation of cytoplasmic TDP-43 aggregates, which were partially detected with anti-phosphorylated TDP-43 antibody

(Fig. 4D). LC3-II and p62 expression levels were not altered by GW4869 treatment (Supplementary Fig. 9A and B), suggesting that this treatment did not cause autophagy dysfunction. Second, we examined the effect of silencing RAB27A by siRNA in Neuro2a cells. RAB27A plays a determinant role in the fusion between MVBs and the plasma membrane (Bobrie *et al.*, 2011) and its silencing has been reported to reduce exosome secretion (Ostrowski *et al.*, 2010; Peinado *et al.*, 2012). Two siRNA oligonucleotides were found to successfully reduce RAB27A protein expression, albeit oligo2 was more efficient (Fig. 4G). RAB27A knockdown reduced exosome secretions (Fig. 4H) and significantly increased insoluble TDP-43 in Neuro2a cells (Fig. 4E and F), in correlation with the knockdown efficiency. In addition, cytoplasmic TDP-43 aggregates were detected in the RAB27A-silenced cells and they were partially phosphorylated (Fig. 4I). These results suggest that exosome secretion is a key pathway for the clearance of TDP-43 aggregates.

We have examined whether GW4869 treatment or silencing RAB27A caused alterations in TDP-43 distribution or splicing function. Analysis of cytosol/nuclear extracts from Neuro2a cells revealed that the nuclear TDP-43 level was not changed by either GW4869 treatment or silencing RAB27A, even though both conditions increased levels of aggregated TDP-43 (Supplementary Fig. 10A and C). We also assessed the splicing pattern of the *Sort1* gene, which has been reported to be a target of TDP-43 (Polymenidou *et al.*, 2011). The splicing pattern of *Sort1* was not changed by GW4869 treatment or silencing RAB27A (Supplementary Fig. 10B and D). These results show that inhibition of exosome secretion promoted TDP-43 aggregation but without causing loss of TDP-43 nuclear function, at least during the time period of these experiments.

## Inhibition of exosome secretion exacerbated the phenotypes of TDP-43$^{A315T}$ transgenic mice

As inhibition of exosome secretion induced formation of TDP-43 aggregates in Neuro2a cells, we further examined the effects of GW4869 in transgenic mice expressing genomic fragments encoding mutant TDP-43$^{A315T}$. The compound GW4869 was administrated intraperitoneally twice a week (60 μg in 200 μl vehicle) in TDP-43$^{A315T}$ mice and control littermates from 20 to 42 weeks old. We chose this protocol based on a previous study in which mice were injected at GW4869 every 48 h for 6 weeks without obvious adverse effects (Dinkins *et al.*, 2014). The control mice were injected with 200 μl vehicle (3.75% DMSO saline). Flotillin-1 levels in exosome fraction from serum and brain were significantly reduced by 65% and 81%, respectively, at 4 h after GW4869 injection (Fig. 5A and B). A reduction in exosome lasted 24 h after the injection (Fig. 5C), although it was not significant at that time (37% reduction). The treated mice had not showed an

apparent behavioural problem during the observation period, and this treatment did not affect their body weights (Supplementary Fig. 11). Yet, the treatment group of male TDP-43$^{A315T}$ mice exhibited a gradual decrease in rotarod performance compared with the non-treatment group (Fig. 5D). Neither the female TDP-43$^{A315T}$ mice (Fig. 5E) nor wild-type mice of both sex (Fig. 5F and G) exhibited a different rotarod performance between treatment and non-treatment groups. We then examined the cognitive deficits of these mice using the novel object recognition test. Control wild-type and TDP-43$^{A315T}$ mice investigated two identical objects equally at the training day (Fig. 5H and J). On the next day, we replaced one object with a different novel object. The wild-type mice spent more time with the novel object than with the familiar object and this behaviour was not affected by GW4869 treatment (Fig. 5K). Non-treated TDP-43$^{A315T}$ mice also spent a longer time with the novel object than the familiar object (Fig. 5I), albeit at lower extent than wild-type mice. In contrast, GW4869-treated TDP-43$^{A315T}$ mice investigated the two objects equally (Fig. 5I) implying that these mice had recognition memory deficit. The results indicate that GW4869 treatment exaggerated the abnormal behavioural phenotypes of TDP-43$^{A315T}$ mice. We analysed male and female mice in this recognition test and there was no sex difference in the results.

## Inhibition of exosome secretion increased TDP-43 aggregation and muscle denervation in TDP-43$^{A315T}$ mice

Immunoblots of CNS extracts from 42-week-old mice showed that GW4869 treatment increased insoluble TDP-43 in the brain and spinal cord of TDP-43$^{A315T}$ mice (Fig. 6A), whereas there was no difference between treatment and non-treatment groups of wild-type mice (Fig. 6B). Immunofluorescence microscopy revealed phosphorylated TDP-43 in cytoplasmic aggregates of CA3 pyramidal neurons from GW4869-treated TDP-43$^{A315T}$ mouse, but not in non-treated TDP-43$^{A315T}$ mouse (Fig. 6C and D). The phosphorylated TDP-43 cytoplasmic aggregates were also seen in spinal motor neurons of GW4869-treated TDP-43$^{A315T}$ mice (arrows in Fig. 6E and F). An antibody against non-phosphorylated TDP-43 also detected diffuse cytoplasmic redistribution of TDP-43 in motor neurons of the treated TDP-43$^{A315T}$ mice (Fig. 6F).

The evaluation of lumbar spinal motor neurons did not show motor neuron loss even in GW4869-treated TDP-43$^{A315T}$ mice (Supplementary Fig. 12). However, complete or partial denervated neuromuscular junctions were increased by GW4869 treatment in TDP-43$^{A315T}$ mice (Fig. 6G and H). Denervated neuromuscular junctions barely occurred in GW4869-treated wild-type mice (Fig. 6G and H). Furthermore, small atrophic muscle fibres were prominent in GW4869-treated TDP-43 $^{A315T}$
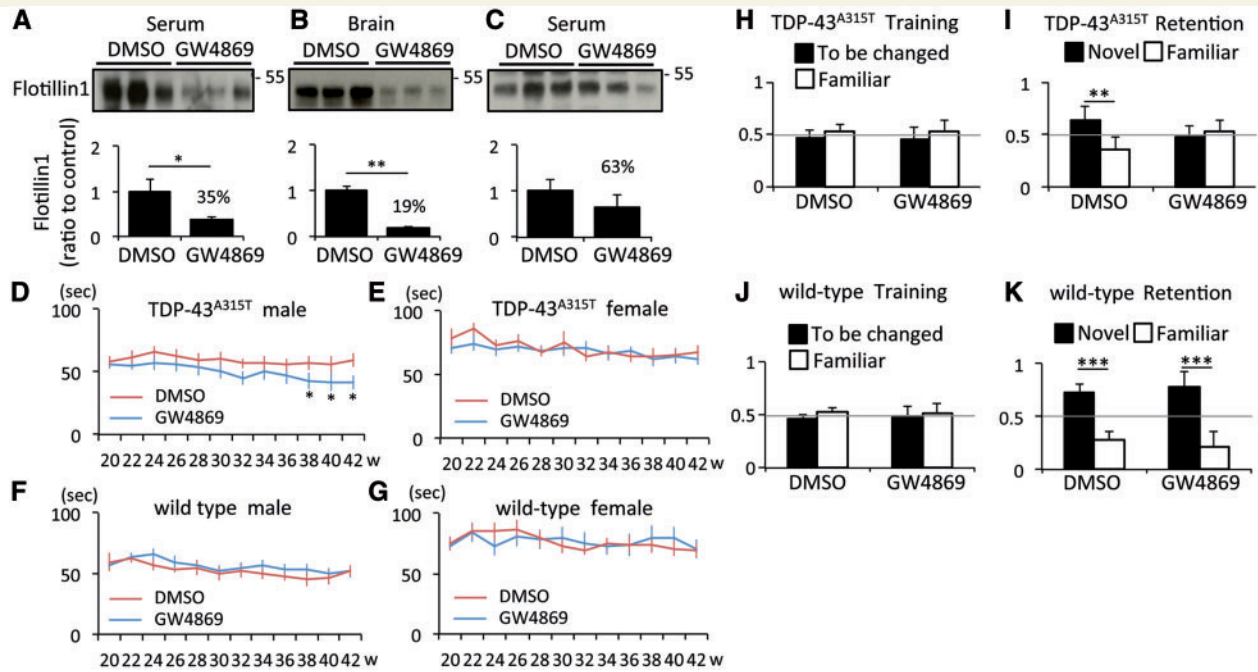
**Figure 5 GW4869 treatment exacerbated TDP-43$^{A315T}$ mouse phenotype. (A and B)** Immunoblots of serum and brain exosomes from six independent wild-type mice 4 h after the intraperitoneal injection of DMSO or GW4869, and densitometric quantification of flotillin I ($n$ = 3 for each group, *$P$ < 0.05, and **$P$ < 0.01, unpaired Student's $t$-test). Error bars indicate SD. **(C)** Immunoblots of serum exosomes from six independent wild-type mice 24 h after the injection of DMSO or GW4869, and densitometric quantification of Flotillin-1 ($n$ = 3 for each group). Error bars indicate SD. **(D–G)** Latency to fall in rotarod task. **(D)** Male TDP-43$^{A315T}$ mice treated with DMSO ($n$ = 12) or GW4869 ($n$ = 13) (*$P$ < 0.05, unpaired Student's $t$-test). **(E)** Female TDP-43$^{A315T}$ mice treated with DMSO ($n$ = 12) or GW4869 ($n$ = 11). **(F)** Male wild-type mice treated with DMSO ($n$ = 8) or GW4869 ($n$ = 10). **(G)** Female wild-type mice treated with DMSO ($n$ = 12) or GW4869 ($n$ = 15). Error bars indicate SEM. **(H–K)** Novel object recognition test. **(H and I)** Data of second day **(H)** or third day **(I)** of TDP-43$^{A315T}$ mice treated with DMSO ($n$ = 12) or GW4869 ($n$ = 13) (**$P$ < 0.01, unpaired Student's $t$-test). **(J and K)** Data of second day **(J)** or third day **(K)** of wild-type mice treated with DMSO ($n$ = 14) or GW4869 ($n$ = 16) (***$P$ < 0.001, unpaired Student's $t$-test). Error bars indicate SD.

mouse (Fig. 6K) compared with non-treated TDP-43 $^{A315T}$ mouse (Fig. 6L) or wild-type mice (non-treated; Fig. 6I, treated; Fig. 6J). Mean muscle fibre size of TDP-43 $^{A315T}$ mice was decreased by GW4869 treatment whereas wild-type mice were not affected with this treatment (Fig. 6M). The analyses of neuromuscular junction and muscle fibre size were carried out with samples from male and female TDP-43$^{A315T}$ mice, and there was no gender difference.

# Discussion

Exosomes are extracellular vesicles secreted from a variety of cell types including neurons, astrocytes, and microglial cells. They contribute to cell-to-cell communication by delivering functional proteins, mRNAs, and miRNAs to recipient cells (Valadi et al., 2007). In addition, accumulating evidence suggest that exosomes contribute to propagation of pathological proteins in neurodegenerative diseases. Exosomes bearing scrapie prion protein (PrP$^{sc}$) can act as a seed of prion propagation (Fevrier et al., 2004; Vella et al., 2007, 2008). In addition, disease-causative proteins

with abnormal modification such as phosphorylated tau, α-synuclein oligomer, or misfolded SOD1 are secreted in association with exosomes (Danzer et al., 2012; Saman et al., 2012; Grad et al., 2014; Asai et al., 2015; Bliederhaeuser et al., 2016).

Here we report that TDP-43 can be secreted via exosomes from neuronal cells and primary neurons. We found that either oxidative stress with ethacrynic acid or proteasome inhibition by MG132 induced TDP-43 cytoplasmic aggregations and increased exosomal TDP-43 secretion. Furthermore, the levels of exosomal TDP-43 were increased in ALS brains, where insoluble phosphorylated TDP-43 pathologies exist, compared to control brains. It is noteworthy that the exosomal TDP-43 from ALS brain was recovered in the soluble fraction, not the insoluble fraction. This is in contrast with the considerable amount of exosomal TDP-43 recovered in the insoluble fraction after treatment of Neuro2a cells with ethacrynic acid or MG132. Thus, the pathological condition occurring in ALS may differ from that of cultured cell models of acute stress. The enhanced levels of soluble and non-phosphory-lated TDP-43 in exosomes from ALS brains suggest that
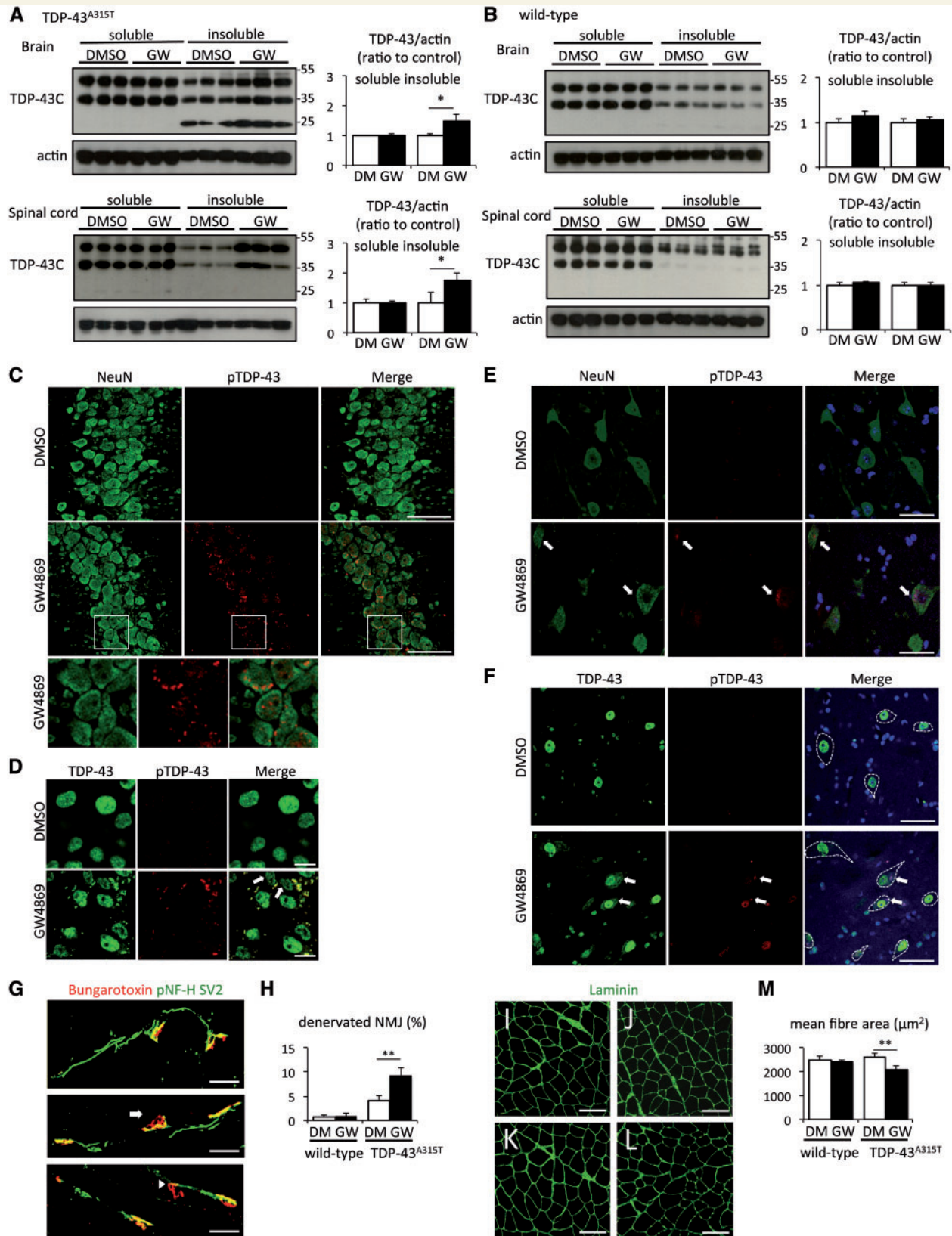
**Figure 6 GW4869 treatment induced TDP-43 pathological modification and muscle denervation.** (**A**) Immunoblots of RIPA-soluble or -insoluble brain/spinal cord fraction from six independent TDP-43$^{A315T}$ mice treated with DMSO or GW4869, and densitometric quantification (*n* = 3 for each group, *P < 0.05, unpaired Student's *t*-test). Error bars indicate SD. (**B**) Immunoblots of RIPA-soluble or -insoluble brain/spinal cord fraction from six independent wild-type mice treated with DMSO or GW4869, and densitometric quantification (*n* = 3 for each group). Error bars indicate SD. (**C** and **D**) Immunofluorescent images of CA3 hippocampal region of TDP-43$^{A315T}$ mouse treated with DMSO or

exosomal TDP-43 fraction was not contaminated by free TDP-43 aggregates during purification. Nonetheless, the possibility that low amount of other particles contaminated the exosome fraction of the brain cannot be excluded. Our analyses revealed massive increases in levels of 15 and 28 kDa TDP-43 C-terminal fragments in exosomes prepared from ALS brains. The C-terminal domain of TDP-43 is involved in the TDP-43 aggregation process (Igaz et al., 2009; Nonaka et al., 2009; Zhang et al., 2009; Fuentealba et al., 2010; Yang et al., 2010; Budini et al., 2012, 2015) and may have a seeding effect (Shimonaka et al., 2016). Hence, the presence of these C-terminal fragments in exosomes may explain why in the present study exosomes derived from ALS brains but not control brains promoted cytoplasmic redistribution of TDP-43 in Neuro2a cells after endocytosis (Fig. 3H–K). Actually, exosomes containing TDP-43 25CTF induced TDP-43 cytoplasmic redistributions as well (Fig. 3L and M). However, the cells neither internalizing ALS brain exosomes nor TDP-43 25CTF-containing exosomes exhibited TDP-43 aggregates. In addition, we did not observe TDP-43 cytoplasmic redistribution in the primary neurons internalized with TDP-43 25CTF-containing exosomes. Thus, our results are only partially supporting a disease model by which TDP-43 proteinopathy may arise and propagate via exosomes.

The autophagy modulations bafilomycin A1 and rapamycin did not change the balance of soluble/insoluble TDP-43 in Neuro2a cells. However, bafilomycin A1 drove exosomal TDP-43 secretion and rapamycin reduced its secretion, suggesting that exosome could play a compensatory role to maintain TDP-43 metabolism. In addition, we also addressed the role of autophagy in exosomal secretion of TDP-43. It is established that autophagy plays an indispensable role in maintenance of protein homeostasis by non-selective or selective removal of cytosolic components such as aggregated proteins and damaged/excess organelles (Mizushima and Komatsu, 2011). Although there is evidence that autophagy has a function in clearance of aggregated TDP-43 (Scotter et al., 2014), autophagy inhibition alone did not induce TDP-43 aggregation in contrast to proteasome inhibition (Urushitani et al., 2010; Wang et al., 2010; Scotter et al., 2014) and as we showed in Fig. 2. Here, we found that autophagy inhibition by

bafilomycin A1 in Neuro2a cells caused increased levels of insoluble TDP-43 in secreted exosomes (Fig. 2), suggesting that exosomal secretion is a compensatory pathway for the clearance of cellular TDP-43 aggregates.

In fact, the suppression of exosome secretion by either GW4869 treatment or RAB27A knockdown induced aggregation of TDP-43 in Neuro2a cells (Fig. 4). When administered to TDP-43$^{A315T}$ transgenic mice, GW4869 also increased insoluble TDP-43 and cytoplasmic aggregation of TDP-43 in neurons (Fig. 6). The inhibition of exosome secretion by GW4869 exacerbated the dysfunction of the motor neuron system and the cognitive deficits in TDP-43$^{A315T}$ mice (Figs 5 and 6). The denervation of neuromuscular junction and the decrease of muscle fibre size occurred similarly in both genders. However, the decline of motor performance by GW4869 treatment was observed only in male TDP-43$^{A315T}$ mice. This apparent gender effect on rotarod test may be related in part to the aged male mice being overweight (Supplementary Fig. 12).

Recent evidence suggests that an efficient autophagic degradation requires functional MVBs (Fader and Colombo, 2009). Knockdown of Tsg101 or VPS24, endosomal sorting complexes required for transport (ESCRT)-I or -III subunit, respectively, was found to cause accumulations of autophagosomes and to induce formation of cytoplasmic TDP-43 aggregates (Filimonenko et al., 2007). The nSMase2 inhibitor GW4869 possibly inhibits MVBs biogenesis because ceramide is a component of MVBs as well as of exosomes. Nonetheless, GW4869 treatment did not change expression levels of LC3-II or p62/SQSTM1 in Neuro2a cells or the CNS of mice (Supplementary Fig. 9A and B), indicating that formation of TDP-43 aggregates by GW4869 treatment did not result from autophagy dysregulation.

Exosome-mediated transfer of pathological proteins in neurodegeneration is emerging as a general mechanism of disease propagation and reducing exosome secretion pharmacologically has been considered as potential therapeutic approach to slow down disease progression. Recent studies with animal models provided evidence of beneficial effects of reducing exosome secretion with GW4869 on amyloid plaque load (Dinkins et al., 2014) and on tau pathology (Asai et al., 2015). However, such 'putative

**Figure 6 Continued**
GW4869 using NeurN (green) and phosphoTDP-43 ser409/410 (red) antibodies (**C**) or TDP-43 (green) and phosphoTDP-43 ser409/410 (red) antibodies (**D**). Scale bars = 50 μm (**C**) or 10 μm (**D**). (**E** and **F**) Immunofluorescent images of spinal cord of TDP-43$^{A315T}$ mouse treated with DMSO or GW4869 using NeurN (green), phosphoTDP-43 ser409/410 (red) antibodies, and DAPI (blue) (**E**), or TDP-43 (green), phosphoTDP-43 ser409/410 (red) antibodies, and DAPI (blue) (**F**). Arrows indicate TDP-43 cytoplasmic aggregates, and dotted lines indicate boundaries of motor neuron. Scale bars = 50 μm. (**G**) Representative immunofluorescent images of neuromuscular junction (NMJ) (pNF-H and SV2; green, bungarotoxin; red). Arrow indicates partially denervated neuromuscular junction and arrowhead indicates totally denervated neuromuscular junction. (**H**) Percentage of partially or totally denervated neuromuscular junction of wild-type or TDP-43$^{A315T}$ mice treated with DMSO or GW4869 (n = 3 for wild-type mouse group, and n = 6 for TDP-43$^{A315T}$ mouse group **P < 0.01, unpaired Student's t-test). Error bars indicate SD. (**I–L**) Immunofluorescent images of gastrocnemius muscle of wild-type mouse treated with DMSO (**I**) or GW4869 (**J**), and TDP-43$^{A315T}$ mouse treated with DMSO (**K**) or GW4869 (**L**) (green; laminin). (**M**) Analysis of mean fibre size of wild-type or TDP-43$^{A315T}$ mice treated with DMSO or GW4869 (n = 3 for wild-type mouse group, and n = 6 for TDP-43$^{A315T}$ mouse group, **P < 0.01, unpaired Student's t-test). More than 100 muscle fibres were measured for each mouse. Error bars indicate SD.

treatment' should be considered with caution as we report here that blocking exosome production with GW4869 induced TDP-43 aggregation, and it exacerbated behavioural and pathological defects in transgenic mice overexpressing low levels of mutant TDP-43[A315T].

In conclusion, our results suggest that excess levels or protein aggregation of TDP-43 in neuronal cells are factors that can promote exosomal secretion of TDP-43 species. A 'prion-like' disease propagation of TDP-43 proteinopathy via secretion and endocytosis of exosomes is in line with our finding that endocytosis of exosomes from ALS brain can provoke cytoplasmic TDP-43 accumulations in recipient cells (Fig. 3H–K). However, treatment strategies in ALS aiming to reduce exosome secretion of TDP-43 might provoke adverse effects based on transgenic mouse data presented here.

# Funding

# Supplementary material

Supplementary material is available at *Brain* online.

# References

Arai T, Hasegawa M, Akiyama H, Ikeda K, Nonaka T, Mori H, et al. TDP-43 is a component of ubiquitin-positive tau-negative inclusions in frontotemporal lobar degeneration and amyotrophic lateral sclerosis. Biochem Biophys Res Commun 2006; 351: 602–11.

Asai H, Ikezu S, Tsunoda S, Medalla M, Luebke J, Haydar T, et al. Depletion of microglia and inhibition of exosome synthesis halt tau propagation. Nat Neurosci 2015; 18: 1584–93.

Bliederhaeuser C, Grozdanov V, Speidel A, Zondler L, Ruf WP, Bayer H, et al. Age-dependent defects of alpha-synuclein oligomer uptake in microglia and monocytes. Acta Neuropathol 2016; 131: 379–91.

Blokhuis AM, Groen EJ, Koppers M, van den Berg LH, Pasterkamp RJ. Protein aggregation in amyotrophic lateral sclerosis. Acta Neuropathol 2013; 125: 777–94.

Bobrie A, Colombo M, Raposo G, Thery C. Exosome secretion: molecular mechanisms and roles in immune responses. Traffic 2011; 12: 1659–68.

Brettschneider J, Arai K, Del Tredici K, Toledo JB, Robinson JL, Lee EB, et al. TDP-43 pathology and neuronal loss in amyotrophic lateral sclerosis spinal cord. Acta Neuropathol 2014; 128: 423–37.

Budini M, Buratti E, Stuani C, Guarnaccia C, Romano V, De Conti L, et al. Cellular model of TAR DNA-binding protein 43 (TDP-43) aggregation based on its C-terminal Gln/Asn-rich region. J Biol Chem 2012; 287: 7512–25.

Budini M, Romano V, Quadri Z, Buratti E, Baralle FE. TDP-43 loss of cellular function through aggregation requires additional structural determinants beyond its C-terminal Q/N prion-like domain. Hum Mol Genet 2015; 24: 9–20.

Danzer KM, Kranich LR, Ruf WP, Cagsal-Getkin O, Winslow AR, Zhu L, et al. Exosomal cell-to-cell transmission of alpha synuclein oligomers. Mol Neurodegener 2012; 7: 42.

Ding X, Ma M, Teng J, Teng RK, Zhou S, Yin J, et al. Exposure to ALS-FTD-CSF generates TDP-43 aggregates in glioblastoma cells through exosomes and TNTs-like structure. Oncotarget 2015; 6: 24178–91.

Dinkins MB, Dasgupta S, Wang G, Zhu G, Bieberich E. Exosome reduction in vivo is associated with lower amyloid plaque load in the 5XFAD mouse model of Alzheimer's disease. Neurobiol Aging 2014; 35: 1792–800.

Fader CM, Colombo MI. Autophagy and multivesicular bodies: two closely related partners. Cell Death Diff 2009; 16: 70–8.

Falsone A, Falsone SF. Legal but lethal: functional protein aggregation at the verge of toxicity. Front Cell Neurosci 2015; 9: 45.

Feiler MS, Strobel B, Freischmidt A, Helferich AM, Kappel J, Brewer BM, et al. TDP-43 is intercellularly transmitted across axon terminals. J Cell Biol 2015; 211: 897–911.

Feneberg E, Steinacker P, Lehnert S, Schneider A, Walther P, Thal DR, et al. Limited role of free TDP-43 as a diagnostic tool in neurodegenerative diseases. Amyotroph Lateral Scler Frontotemporal Degener 2014; 15: 351–6.

Fevrier B, Vilette D, Archer F, Loew D, Faigle W, Vidal M, et al. Cells release prions in association with exosomes. Proc Natl Acad Sci USA 2004; 101: 9683–8.

Filimonenko M, Stuffers S, Raiborg C, Yamamoto A, Malerod L, Fisher EM, et al. Functional multivesicular bodies are required for autophagic clearance of protein aggregates associated with neurodegenerative disease. J Cell Biol 2007; 179: 485–500.

Fuentealba RA, Udan M, Bell S, Wegorzewska I, Shao J, Diamond MI, et al. Interaction with polyglutamine aggregates reveals a Q/N-rich domain in TDP-43. J Biol Chem 2010; 285: 26304–14.

Grad LI, Yerbury JJ, Turner BJ, Guest WC, Pokrishevsky E, O'Neill MA, et al. Intercellular propagated misfolding of wild-type Cu/Zn superoxide dismutase occurs via exosome-dependent and -independent mechanisms. Proc Natl Acad Sci USA 2014; 111: 3620–5.

Hasegawa M, Arai T, Nonaka T, Kametani F, Yoshida M, Hashizume Y, et al. Phosphorylated TDP-43 in frontotemporal lobar degeneration and amyotrophic lateral sclerosis. Ann Neurol 2008; 64: 60–70.

Igaz LM, Kwong LK, Chen-Plotkin A, Winton MJ, Unger TL, Xu Y, et al. Expression of TDP-43 C-terminal fragments in vitro recapitulates pathological features of TDP-43 proteinopathies. J Biol Chem 2009; 284: 8516–24.

Iguchi Y, Katsuno M, Takagi S, Ishigaki S, Niwa J, Hasegawa M, et al. Oxidative stress induced by glutathione depletion reproduces pathological modifications of TDP-43 linked to TDP-43 proteinopathies. Neurobiol Dis 2012; 45: 862–70.

Johnson BS, McCaffery JM, Lindquist S, Gitler AD. A yeast TDP-43 proteinopathy model: exploring the molecular determinants of TDP-43 aggregation and cellular toxicity. Proc Natl Acad Sci USA 2008; 105: 6439–44.

Johnson BS, Snead D, Lee JJ, McCaffery JM, Shorter J, Gitler AD. TDP-43 is intrinsically aggregation-prone, and amyotrophic lateral sclerosis-linked mutations accelerate aggregation and increase toxicity. J Biol Chem 2009; 284: 20329–39.

Lasser C, Eldh M, Lotvall J. Isolation and characterization of RNA–containing exosomes. J Vis Exp 2012; 59: e3037.

Lee HH, Elia N, Ghirlando R, Lippincott-Schwartz J, Hurley JH. Midbody targeting of the ESCRT machinery by a noncanonical coiled coil in CEP55. Science 2008; 322: 576–80.

Ling SC, Albuquerque CP, Han JS, Lagier-Tourenne C, Tokunaga S, Zhou H, et al. ALS-associated mutations in TDP-43 increase its stability and promote TDP-43 complexes with FUS/TLS. Proc Natl Acad Sci USA 2010; 107: 13318–23.

Ling SC, Polymenidou M, Cleveland DW. Converging mechanisms in ALS and FTD: disrupted RNA and protein homeostasis. Neuron 2013; 79: 416–38.

Maniecka Z, Polymenidou M. From nucleation to widespread propagation: a prion-like concept for ALS. Virus Res 2015; 207: 94–105.

Mizushima N, Komatsu M. Autophagy: renovation of cells and tissues. Cell 2011; 147: 728–41.

Neumann M, Sampathu DM, Kwong LK, Truax AC, Micsenyi MC, Chou TT, et al. Ubiquitinated TDP-43 in frontotemporal lobar degeneration and amyotrophic lateral sclerosis. Science 2006; 314: 130–3.

Nonaka T, Kametani F, Arai T, Akiyama H, Hasegawa M. Truncation and pathogenic mutations facilitate the formation of intracellular aggregates of TDP-43. Hum Mol Genet 2009; 18: 3353–64.

Nonaka T, Masuda-Suzukake M, Arai T, Hasegawa Y, Akatsu H, Obi T, et al. Prion-like properties of pathological TDP-43 aggregates from diseased brains. Cell Rep 2013; 4: 124–34.

Ostrowski M, Carmo NB, Krumeich S, Fanget I, Raposo G, Savina A, et al. Rab27a and Rab27b control different steps of the exosome secretion pathway. Nat Cell Biol 2010; 12: 19–30; 1–13.

Peinado H, Aleckovic M, Lavotshkin S, Matei I, Costa-Silva B, Moreno-Bueno G, et al. Melanoma exosomes educate bone marrow progenitor cells toward a pro-metastatic phenotype through MET. Nat Med 2012; 18: 883–91.

Perez-Gonzalez R, Gauthier SA, Kumar A, Levy E. The exosome secretory pathway transports amyloid precursor protein carboxyl-terminal fragments from the cell into the brain extracellular space. J Biol Chem 2012; 287: 43108–15.

Polymenidou M, Lagier-Tourenne C, Hutt KR, Huelga SC, Moran J, Liang TY, et al. Long pre-mRNA depletion and RNA missplicing contribute to neuronal vulnerability from loss of TDP-43. Nat Neurosci 2011; 14: 459–68.

Rajendran L, Honsho M, Zahn TR, Keller P, Geiger KD, Verkade P, et al. Alzheimer's disease beta-amyloid peptides are released in association with exosomes. Proc Natl Acad Sci USA 2006; 103: 11172–7.

Ravits JM, La Spada AR. ALS motor phenotype heterogeneity, focality, and spread: deconstructing motor neuron degeneration. Neurology 2009; 73: 805–11.

Saman S, Kim W, Raya M, Visnick Y, Miro S, Saman S, et al. Exosome-associated tau is secreted in tauopathy models and is selectively phosphorylated in cerebrospinal fluid in early Alzheimer disease. J Biol Chem 2012; 287: 3842–9.

Saura J, Tusell JM, Serratosa J. High-yield isolation of murine microglia by mild trypsinization. Glia 2003; 44: 183–9.

Schneider CA, Rasband WS, Eliceiri KW. NIH Image to ImageJ: 25 years of image analysis. Nat Methods 2012; 9: 671–5.

Scotter EL, Vance C, Nishimura AL, Lee YB, Chen HJ, Urwin H, et al. Differential roles of the ubiquitin proteasome system and autophagy in the clearance of soluble and aggregated TDP-43 species. J Cell Sci 2014; 127: 1263–78.

Shimonaka S, Nonaka T, Suzuki G, Hisanaga SI, Hasegawa M. Templated aggregation of TDP-43 by seeding with TDP-43 peptide fibrils. J Biol Chem 2016; 291: 8896–907.

Swarup V, Phaneuf D, Bareil C, Robertson J, Rouleau GA, Kriz J, et al. Pathological hallmarks of amyotrophic lateral sclerosis/frontotemporal lobar degeneration in transgenic mice produced with TDP-43 genomic fragments. Brain 2011; 134: 2610–26.

Tabatadze N, Savonenko A, Song H, Bandaru VV, Chu M, Haughey NJ. Inhibition of neutral sphingomyelinase-2 perturbs brain sphingolipid balance and spatial memory in mice. J Neurosci Res 2010; 88: 2940–51.

Takagi S, Iguchi Y, Katsuno M, Ishigaki S, Ikenaka K, Fujioka Y, et al. RNP2 of RNA recognition motif 1 plays a central role in the aberrant modification of TDP-43. PloS One 2013; 8: e66966.

Urushitani M, Sato T, Bamba H, Hisa Y, Tooyama I. Synergistic effect between proteasome and autophagosome in the clearance of polyubiquitinated TDP-43. J Neurosci Res 2010; 88: 784–97.

Valadi H, Ekstrom K, Bossios A, Sjostrand M, Lee JJ, Lotvall JO. Exosome-mediated transfer of mRNAs and microRNAs is a novel mechanism of genetic exchange between cells. Nat Cell Biol 2007; 9: 654–9.

Vella LJ, Greenwood DL, Cappai R, Scheerlinck JP, Hill AF. Enrichment of prion protein in exosomes derived from ovine cerebral spinal fluid. Vet Immunol Immunopathol 2008; 124: 385–93.

Vella LJ, Sharples RA, Lawson VA, Masters CL, Cappai R, Hill AF. Packaging of prions into exosomes is associated with a novel pathway of PrP processing. J Pathol 2007; 211: 582–90.

Wang X, Fan H, Ying Z, Li B, Wang H, Wang G. Degradation of TDP-43 and its pathogenic form by autophagy and the ubiquitin-proteasome system. Neurosci Lett 2010; 469: 112–6.

Watanabe S, Kaneko K, Yamanaka K. Accelerated disease onset with stabilized familial amyotrophic lateral sclerosis (ALS)-linked mutant TDP-43 proteins. J Biol Chem 2013; 288: 3641–54.

Yang C, Tan W, Whittle C, Qiu L, Cao L, Akbarian S, et al. The C-terminal TDP-43 fragments have a high aggregation propensity and harm neurons by a dominant-negative mechanism. PloS One 2010; 5: e15878.

Zhang YJ, Xu YF, Cook C, Gendron TF, Roettges P, Link CD, et al. Aberrant cleavage of TDP-43 enhances aggregation and cellular toxicity. Proc Natl Acad Sci USA 2009; 106: 7607–12.